HHS Public Access

Author manuscript

Polym Adv Technol. Author manuscript; available in PMC 2020 May 01.

Published in final edited form as:

Polym Adv Technol. 2019 May ; 30(5): 1189–1197. doi:10.1002/pat.4551.

Load-bearing biodegradable polycaprolactone-poly (lactic-co-glycolic acid)- beta tri-calcium phosphate scaffolds for bone tissue regeneration

Alok Kumar[a], **Yiren Zhang**[b], **Amalia Terracciano**[c], **Xiao Zhao**[b], **Tsan-Liang Su**[c], **Dilhan M. Kalyon**[b], **Sara Katebifar**[d,e], **Sangamesh G. Kumbar**[d,e], **Xiaojun Yu**[a,*]

[a]Department of Biomedical Engineering

[b]Department of Chemical Engineering and Materials Science

[c]Center for Environmental Systems Stevens Institute of Technology, Hoboken, NJ, USA

[d]Department of Biomedical Engineering, University of Connecticut, Storrs, CT, USA

[e]Department of Orthopedic Surgery, University of Connecticut Health, Farmington, CT, USA

Abstract

A biodegradable scaffold with tissue ingrowth and load-bearing capabilities is required to accelerate the healing of bone defects. However, it is difficult to maintain the mechanical properties as well as biodegradability and porosity (necessary for bone ingrowth) at the same time. Therefore, in the present study, polycaprolactone (PCL) and poly(lactic-co-glycolic acid) (PLGA5050) were mixed in varying ratio and incorporated with 20 wt.% βTCP. The mixture was shaped under pressure into originally non-porous cylindrical constructs. It is envisioned that the fabricated constructs will develop porosity with the time-dependent biodegradation of the polymer blend. The mechanical properties will be sustained since the decrease in mechanical properties associated with the dissolution of the PLGA and the formation of the porous structure will be compensated with the new bone formation and ingrowth.

To prove the hypothesis, we have systematically studied the effects of samples composition on the time-dependent dissolution behavior, pore formation, and mechanical properties of the engineered samples, *in vitro*. The highest initial (of as-prepared samples) values of the yield strength (0.021±0.002 GPa) and the Young's modulus (0.829±0.096 GPa) were exhibited by the samples containing 75 wt.% of PLGA. Increase of the PLGA concentration from 25 wt.% to 75 wt.% increased the rate of biodegradation by a factor of 3 upon 2 weeks in phosphate buffered saline (1× PBS). The overall porosity and the pore sizes increased with the dissolution time indicating that the formation of in-situ pores can indeed enable the migration of cells followed by vascularization and bone growth.

Keywords

PCL; PLGA; Biodegradation; Mechanical properties; Bone

[*]Corresponding Author: Xiaojun Yu, PhD. Associate Professor, Department of Biomedical Engineering Stevens Institute of Technology, 1 Castle Point on Hudson, Hoboken, NJ 07030, USA, Ph.: 201.216.5256, Fax: 201.216.8240, xyu@stevens.edu.

1. Introduction

The extent of damage after fracture can affect the self-repair ability of a bone. In this context, as compared to large fracture, small fractures are usually able to heal perfectly [1]. Larger fractures (critical-sized bone defects) are difficult to repair and need a tissue engineering approach and porous scaffold to promote healing. As a general guideline, defect length greater than 50% loss of total circumference of bone is considered as a critical-sized bone defect [2]. Potential candidates for the repair of bone defects are allografts and autografts [3–5]. However, the possible risk of transmission of disease with allografts as well as poor osteoconductivity and mechanical properties limit their wider application [6–8]. Additionally, autografts are limited in supply and a second surgery is needed to harvest the graft, which may delay the recovery of the patient [9]. In contrast, bone tissue engineering (BTE) approach can be adapted to reduce the healing time by accelerating the bone remodeling [10]. Bone remodeling is affected by the properties of scaffolds which include composition, architecture, physical and mechanical properties, and biodegradability [11–13].

Considering the above aspects, a number of related studies have been carried out in the past on different methods for the stimulation of bone regeneration. In these works, researchers have tried to use various materials, such as 3D printed porous metallic scaffolds, metallic foam, 3D printed porous ceramic scaffolds, 3D printed porous polymeric scaffolds, biodegradable polymeric composites, ceramic or polymeric scaffolds created by salt-leaching method or by freeze-drying, to accomplish the required properties for the bone tissue applications [14–16]. For instance, Hollander et al. [17] fabricated the porous scaffolds of titanium alloy (Ti-6Al-4V) using direct laser forming for the bone tissue engineering applications. In a similar work, Pattanayak et al. [18] used selective laser sintering to produce a porous scaffold of titanium, followed by chemical treatment to improve the bioactivity. In addition to 3D printed scaffolds, porous titanium foam produced by the powder metallurgy technique was also found suitable to repair the bone defects [19]. Although these scaffolds possess remarkable mechanical strength, they are non-degradable [20]. Also, the metallic scaffold can produce toxic metal ions due to corrosion [21]. In contrast to metallic materials, porous ceramics or glass scaffolds are degradable [22,23] but, poor in mechanical properties due to the presence of pores [24]. 3D printed polymeric scaffolds with pre-defined pore architectures have advantages due to low-temperatures of fabrication. However, the degradation rate of most of the polymers (e.g., PCL) used in the 3D printing is slow and such scaffolds take 2–4 years to dissolve completely [25]. Although the degradation rate of these scaffolds can be controlled by selecting the blend of two or more polymers with different degradation rates, the poor compressive strength due to the presence of designed pores remains an area of possible improvement [26].

Considering the importance of polymeric biomaterials to address the issue of biodegradability, vascularization[27], and compressive strength, in the present work, biodegradable scaffolds of polycaprolactone-poly(lactic-co-glycolic acid)-beta tri-calcium phosphate (PCL-PLGA- βTCP) were developed. PCL is an FDA approved slow degrading polymer with poor cell adhesion proliferation properties due to hydrophobic property [28]. In contrast, PLGA promotes better cell adhesion due to its hydrophilic nature [28]. However,

PLGA is brittle and exhibits relatively low mechanical strength, while PCL is more ductile in nature [29].

There were three primary reasons behind the synthesis of PCL-PLGA-βTCP scaffolds: (i) development of a densified biodegradable scaffold with improved compressive strength to provide the structural support necessary during the reconstruction of bone defects; (ii) development of a biodegradable scaffold with βTCP ($Ca_3(PO_4)_2$) particles to supplement the defect area with Ca^{2+} and PO_4^{3-}, required to encourage bone regeneration; (iii) development of a scaffold with the ability to form in-situ pores (required for the tissue ingrowth) via the degradation of the faster dissolving polymer component (PLGA5050) from the PCL-PLGA scaffolds at the later stage of implantation.

2. Experimental Procedure

2.1. Materials

Polycaprolactone (PCL, Cat. No. 440744, MW: 80,000, Tg ~ −60 °C) and acid terminated poly(lactic-co-glycolic acid) (PLGA5050, Cat. No. 719900, MW: 38,000–50,000, Tg ~ 46–50 °C) were procured from Sigma Aldrich. Beta tri-calcium phosphate powder (β-TCP, Cat. No. 440744) and 1,1,1,3,3,3-Hexafluoro-2-propanol (HFIP, Cat. No. 003409) were purchased from Fluka and Oakwood Chemicals, respectively.

2.2. Scaffold fabrication

Porous scaffolds of PCL-PLGA-βTCP were prepared by heating the mixture of PCL, PLGA and beta TCP at 150 °C in PTFE mold, followed by compression as shown in Figure 1. For this, first PCL and PLGA were mixed in at various ratios (x and y, respectively) to make 100 wt.%. After that, 20 wt.% beta TCP of total weight (of PCL and PLGA) was added to make xPCL-yPLGA-20βTCP compositions. Based on various trials, three compositions (weight percent ratio) were selected for the studies: 25PCL-75PLGA-20βTCP (PA75), 50PCL-50PLGA-20βTCP (PA50), 75PCL-25PLGA-20βTCP (PA25). At least three samples of each composition were used to obtain the statistically relevant data.

For the sample preparation, PCL, PLGA5050, and βTCP were mixed at the ratios mentioned above (25:75:20, 50:50:20, and 75:25:20), followed by the transfer of this mixture into a cylindrical-shaped (6 mm diameter, 12 mm height) PTFE mold. The material was compressed to full density and heated for 15 min at 150 °C in air. After the completion of the heating cycle, samples were removed from the furnace and further compressed to full density, and extra material (a mixture of PCL, PLGA5050, and βTCP) was added if required. These samples were again heated for 15 min at 150 °C in air and compressed to full density at the end of the heating cycle. After the completion of the second heating cycle, samples were heated again for 1 min without any further compression to relieve the stresses generated in the samples due to compression, followed by furnace cooling. Extra material from the as-prepared scaffolds was cleaned using a scalpel.

All the as-prepared samples were washed (sterilized) in 100% ethanol three times, 2 min each. Dried samples were stored at room temperature sealed in glass tubes until further characterization.

2.3. Phase and Microstructural Characterization

X-ray diffraction (XRD) of as-sintered samples was carried out to study the phase transformation during fabrication. For all three PCL-PLGA-beta TCP samples similar processing conditions were used. Accordingly, we have only presented the XRD of PA50, as a representative phase assemblage data. For this, an X-ray diffractometer (Ultima IV, Rigaku, USA), operated at 40 kV and 30 mA with Cu K_α radiation (λ = 0.15418 nm) was used in the 2θ range of 10°−90°. For the data collection, an incident angle of 5° was selected with a step size of 0.02° and a scanning rate of 2°/min. For the beta TCP data analysis, International Center for Diffraction Data (ICDD) standard (pdf # 32–0176) was used. For the topography and microstructural characterization, sintered samples were analyzed using scanning electron microscope (SEM, Auriga 40, Zeiss, Germany), operated at an accelerating voltage of 10 kV and a working distance of 10 mm. Furthermore, energy dispersive spectroscopy (EDS, X-Max, Oxford Instruments, UK) mapping was used for the composition analysis and to confirm the distribution of beta TCP in the sample. Prior to SEM/EDS samples were gold coated (EM MED020, Leica, Germany) to minimize the charging effect. For the pore architecture analysis, samples before and after the dissolution studies were observed using stereo microscope (SMG1500, Nikon, Japan).

Furthermore, differential scanning calorimetry (DSC, Q100, TA Instruments, USA) was carried out between 0 °C to 100 °C at a heating rate of 10 °C/min under a nitrogen atmosphere to evaluate the effects of the processing conditions on the glass transition temperature of the PCL and PLGA as well as PCL-PLGA blend. Melting (Tm) and glass transition (Tg) temperatures were measured from the peak of the melting endotherms and from the inflection point of the specific heat capacity, respectively. The area under the peak was calculated to obtain the enthalpy of fusion (ΔHm), and the data were used to calculate the percentage degree of crystallinity degree (%Xc) using the following equation [30].

$$X_C(\%) = \left(\frac{\Delta H_m}{\left(\frac{f_{PCL}}{f_{PCL} + f_{PLGA}} \right) \times \Delta H_m^0} \right) \times 100 \quad (1)$$

where ΔH_m = experimental melting enthalpy (fusion)

ΔH^0_m = enthalpy of 100% crystalline material = 136 J/g for the PCL [30]

w = weight fraction of material

2.4. Density and porosity

The liquid displacement method was used for the measurement of the density and percentage porosity. In this measurement, ethanol was used instead of water, because ethanol can easily penetrate the pores and did not induce shrinkage or swelling. Briefly, the weight of a dry sample (W) was recorded. This sample was immersed in a cylinder containing a known volume (V1) of 100% ethanol. The sample was kept in ethanol for 5 min, and during this time a series of brief evacuation– repressurization cycles were conducted to force the ethanol into the pores of the sample. This evacuation– repressurization cycles were

continued until no air bubbles were observed evolving from the sample. After this, the volume of ethanol (V2) was recorded. The sample was removed from ethanol and the volume of the residual ethanol remaining in the measuring cylinder was noted (V3). The volume of the sample without pores was equivalent to V2 − V1, and pore volume was available from V1 − V3. Therefore, the total volume of the sample (V) can be estimated using the formula: (V2 − V1) + (V1− V3) = V2 − V3. The density of the sample (d) can be expressed as: W/V, and the percentage porosity of the sample can be calculated using the formula: [(V1 − V3)/V]×100.

2.5. Mechanical Properties

The deformation behavior of the sintered samples was studied to estimate the elastic modulus, 0.2% yield strength, and Young's modulus. For the testing, a universal testing machine (5581, Instron, USA) was used in the compression mode for the mechanical testing of materials. For the compression, cylindrical samples of 6 mm in diameter, 12 mm in height were prepared and tested at a speed of 1.3 mm/min.

2.6. Scaffold stability in aqueous conditions

After measuring the weight of as-sintered samples, samples were cleaned in 100% ethanol and dried in air, followed by UV irradiation for 30 min. Each cylindrical sample (12 mm × 6 mm) was transferred to the 4 ml 1×PBS and kept under agitation at 37 °C for 2, 4, 6, 8, 16, 24, and 48 weeks. After the dissolution, samples were removed from the solution, and the pH of the solution was recorded. Removed samples were carefully washed in deionized water three times for 2 min each on a shaker. Washed samples were stored at −80 °C for 24 h and freeze-dried (FreeZone, Labconco, USA) afterward. Dimension and weight of freeze-dried samples were measured, followed by sample and pore volume calculation using liquid displacement method. Collected data were analyzed using the weights of starting samples (before dissolution) to calculate the weight loss and change in the pore volume using the following equation:

$$\textit{Change}\ \text{in the porosity}\ (\%) = \left(\frac{V_i - V_f}{V_i}\right) \times 100 \tag{2}$$

where Vi = total volume of the sample before the dissolution

Vf = total volume of the sample after the dissolution

2.7. Statistical analysis

The obtained mechanical properties and dissolution data were analyzed using a commercially available statistical analysis software (SPSS, IBM, USA). A Post-hoc test (multivariate comparison) was used to compare the mean values. The two way ANOVA (Analysis of Variance) with Dunnett C test was used to assess the significant difference among the samples mean at $p < 0.05$ (p is the probability when there is no difference exists between the samples mean). Data were presented as mean ± standard error of the mean.

3. Results

3.1. Microstructure and Physical Properties

As-sintered scaffolds of 25PCL-75PLGA-20βTCP, 50PCL-50PLGA-20βTCP, and 75PCL-25PLGA-20βTCP were studied under an optical microscope and were determined to consist of solid cylinders with no visible surface pores. PLGA was noted to be present at the boundaries of PCL particles. The SEM analysis carried out in secondary electron mode revealed a rough surface with a strong interface between PCL and PLGA phases (Figure 2). Micrographs of the surfaces of the samples obtained under higher magnifications revealed the presence of microcracks.

The measured densities of PA75, PA50, and PA25 samples were ~ 1.3 g/cm^3, ~ 0.77 g/cm^3, and ~ 0.84 g/cm^3, respectively. The percentage porosity of the PA75, PA50, and PA25 of the as-sintered samples were ~ 20, ~ 28.4, and ~ 47.7 with no open pores visible.

The glass transition temperature of the PCL [31] and PLGA were −60 °C and 38 °C, respectively (Supplementary Figure 1). For the monolithic PCL sample, the enthalpy of fusion and crystallinity were 54.16 J/g and 39.8 %, respectively. DSC results confirmed the semicrystalline nature of PCL and the amorphous nature of PLGA5050. As compared to monolithic PCL, the results showed a higher crystallinity of 50PCL-50PLGA-20βTCP samples (51.9 %) with an enthalpy of fusion of 35.32 J/g.

3.2. Phase Assemblage

The XRD pattern of as-sintered PA50 is presented in Figure 3. A comparison with the ICDD database, XRD result confirmed the presence of beta TCP, with the peaks associated with beta TCP marked in Figure 3 with solid diamond symbols. Furthermore, the comparison of the diffraction pattern with the existing literature [32], confirmed the presence of the PCL phase (peaks associated with PCL are marked with solid circles). Importantly, no distinct peaks associated with PLGA [33] were observed except one broad peak extended from 10° −25°. Furthermore, the detailed EDS mapping of as-sintered samples confirmed the presence of Ca, P, O, and C in the PCL-PLGA matrix (Figure 4, Supplementary Figures 2a and 2b).

3.3. Mechanical Properties

The compression testing data of sintered samples, PA75, PA50, and PA25 are presented in Figures 5A, 5B, and 5C, respectively. Figure 5D shows the values of 0.2% yield strength and Young's modulus, that were determined from the stress-strain curve. The obtained data are presented as a mean ± standard error of the mean. The compression testing of scaffolds at room temperature showed a significant effect of the PCL over the PLGA weight ratio on the yield strength and Young's modulus (Figure 5D). The 0.2% yield strength values for the PA75, PA50 and PA25 samples were 0.021±0.002, 0.0120±0.003, and 0.01±0.001 GPa, respectively. The values of Young's modulus were 0.829±0.096, 0.335±0.014, and 0.238±0.2 GPa, respectively. Stress-strain curve exhibited an increasing trend of the compressive stress to reach a maximum value of 0.023 GPa in the case of high PLGA samples (PA75) and thereafter, a decrease in compressive stress. In contrast, in the cases of PA50 and PA25, an increasing trend in the compressive stress was noted. As compared to

PA25 (~ 0.020 GPa), the compressive stress values were higher in the case of PA50 (~ 0.025 GPa) at the maximum applied strain of 0.3. Statistical analysis showed the significant difference (at $p < 0.05$) between PA75 and PA25 samples for the 0.2% yield strength and Young's modulus data. However, no statistically significant difference was noted when PA75 and PA50, as well as PA50 and PA25 samples, were compared for 0.2% yield strength and Young's modulus. Visual observation of PA75 samples during the compression testing revealed the crack initiation at the upper end of samples (upper ram/loading side) with fracture along the axis of samples. In contrasts, the fracture was in the transverse direction in the case of PA25 samples with smaller deformations observed for PA75. Importantly, bending in the samples was noted during the compression of PA75. In the case of PA50 samples, the average of both axial and transverse deformation behavior of the PA75 and PA25 were observed with no apparent bending.

3.4. Stability of scaffolds in the aqueous conditions

The results of the dissolution study of the samples in 1×PBS are shown in Figure 6 and 7. Figure 6A shows the percentage weight loss as a function of dissolution time and Figure 6B shows the rate of dissolution as a function of time. Figure 7 shows the percentage porosity as a function of time. Figure 6 points to the determining role of PLGA5050 on the degradation of PCL-PLGA scaffolds. The experimental data reported in Figure 6 and 7 are presented as mean ± standard error of the mean. A higher percentage weight loss was found in the case of scaffolds with a higher amount of PLGA5050 (Figure 6A). An increase of the PLGA concentration from 25 wt.% to 50 wt.% increased the rate of biodegradation by a factor of 2 upon 2 weeks of dissolution (Figure 6B). Furthermore, a threefold increase in the rate of biodegradation was noted with the increase of the PLGA concentration from 25 wt.% to 75 wt.%. The rate of degradation was highest at 4 weeks, and thereafter, the rate of degradation diminished. Statistical analysis (at $p < 0.05$) of the data confirmed a statistically significant difference when 2 weeks (%weight loss) samples were compared with 4, 6, 8, 16, and 24 weeks, irrespective of the sample compositions. No statistically significant differences were noted when samples of 4, 6, 8, 16, and 24 weeks dissolution were compared with each other. Importantly, stereo-microscopic observation (data not shown) did not reveal the presence of any surface pores until 2 weeks of dissolution study. However, samples after 4 weeks of dissolution exhibited pores, specifically, located at the boundaries of PCL particles. The calculation of the volume of samples before and after the dissolution study revealed an increase in porosity with time (Figure 7). Results indicated a ~13% increase in the porosity of PA75 samples after 2 weeks of dissolution. However, in the case of PA50 and PA25, the corresponding increases in porosity was ~17% and ~6%, respectively. After 2 weeks, excessive degradation of PLGA led to the disintegration of samples for PA75, while PA50 and PA25 samples were intact. Therefore, no data were available for PA75 after 2 weeks. In the case of PA50, we noted a disintegration in samples after 8 weeks. However, no such breakup of the samples was noted in case of PA25 samples until 24 weeks of dissolution, for which the maximum created porosity was 15%. For PA50 samples, the value of porosity was ~23% and ~35% for 4 and 6 weeks, respectively. For PA50, no significant changes in porosity were noted when 8 weeks of samples were compared with 6 weeks of samples at $p < 0.05$. As compared to PA25 and PA50 samples, a minimal dissolution was noted in case of

PA25 samples. However, no statistically significant difference (at $p < 0.05$) were noted among the samples for the different duration of dissolution (2, 4, 6, 8, 16, and 24).

4. Discussion

Scaffolds with designed porosity can be promising graft materials for bone regeneration due to the presence of interconnected pores, required for the neovascularization [12]. However, scaffolds with high porosity also exhibit lower compressive strengths [26]. Therefore, it is difficult to design a highly porous scaffold with acceptable mechanical properties at the same time. Apart from this, biodegradable biomaterials are identified as an ideal substrate material for bone growth, because these biomaterials provide the structural stability that is necessary during the implantation and progressive degradation of these materials while providing the additional requisite volume for bone growth. Considering the inherent complexity (e.g., microstructure, pore architecture, composition, strength, biodegradability) required in an ideal scaffold for bone tissue engineering, composite scaffolds of blends of two biodegradable materials (PCL-PLGA-βTCP) were fabricated to serve for load-bearing bone defects.

The scaffolds were characterized by a dense structure with no visible pores upon fabrication (Figure 1). It is anticipated that the fabricated constructs will develop porosity during the biodegradation of the polymer blend (PCL-PLGA-beta TCP), i.e., with the PLGA biodegrading faster in comparison to PCL so that the volume occupied by PLGA is converted into a porous network with time. As discussed before, the absence of pores during the implantation is expected to improve the mechanical properties. The unique composition of the designed scaffold is expected to play an important role in the healing phase. For instance, the overall structure will provide mechanical support to the defect area and help in maintaining the length of the affected limb. The degradation of PLGA5050 will help in the release of βTCP (source of Ca^{2+} and PO_4^{3-}) into the defect site, required for the new bone mineralization. Furthermore, due to slow degradation of PCL (can take up to 1 year to degrade [34]), the fast dissolution of PLGA (PLGA5050 can completely degrade in around 4 weeks [35]) will leave the porous PCL skeleton without significant loss in the scaffold shape and size. This is required to maintain the structural integrity and the length of the affected limb. The newly formed pore channels in the PCL skeleton will help in the formation of the vascular network and therefore, facilitate the supply of oxygen and nutrients to the cells growing deep inside the scaffolds [36].

Characterization of samples (PA75, PA50, and PA25) confirmed densities that are in the range of those of cancellous bone (0.1–1.0 g/cm^3) [37]. Furthermore, the rough surface as apparent from the SEM is expected to play an important positive role during cell adhesion and proliferation (Figure 2) [38]. The XRD results confirmed the presence of all three phases in the samples without any detrimental effect of processing on the PCL, PLGA5050, and β-TCP (Figure 3). The presence of sharp peaks corresponding to beta TCP and PCL confirmed the crystalline nature of these materials. However, the broad peak at 10°−25° is related to the amorphous phase of PLGA5050. The presence of all three elements Ca, P, and O in the EDS map is a confirmation of the uniform distribution of beta TCP in the samples (Figure 4).

Importantly, C was detected in the entire map area which corresponds to the polymeric (PCL-PLGA) matrix.

Compression testing is widely used to measure the mechanical properties of the biomaterials for orthopedic applications. It is important to mention that the PCL is ductile, while PLGA is brittle at room temperature [28]. This is due to the glass transition temperature, which is below the room temperature for the PCL (- 60 °C) and above the room temperature for the PLGA (40–60 °C). A clear effect of this was noticed in the yield strength and Young's modulus values of the samples (Figure 5). The higher yield strength and Young's modulus values of PA75 samples versus those of PA25 and PA50 is mainly due to the presence of PLGA. The behavior of samples during the compression testing was directly correlated with the composition and the presence of microcracks in the as-prepared samples. For instance, initial increase and thereafter sudden decrease in the stress value in case of P75 samples is related to the brittle fracture in PLGA phase. A higher stress value in case of PA50 is a result of PLGA phase. A continuous increase in the stress value during the compression testing of PA50 and PA25 is correlated with ductile PCL. Therefore, change in the PCL, and PLGA ratio can significantly affect the mechanical properties of the PCL-PLGA composites. In this perspective, the use of a slow degradable phase with a glass transition temperature above the body temperature can significantly increase the lifetime of the scaffold in a load-bearing application.

Biodegradation of the scaffold and the sustained release of calcium are very important to support the natural bone repair process. After providing initial structural stability, the biodegradation of scaffold may allow the blood vessels to grow inside the newly formed pores (due to degradation of PLGA5050 from the PCL matrix) [39]. Furthermore, the degradation of scaffolds is expected to provide the space for the bone growth, *in vivo* [12]. This was confirmed from the porosity data, in which an increase in the percentage porosity with time was noted in the case of PA75, PA50, and PA25 samples (Figure 7). The PA50 scaffolds were characterized by a high percentage of porosity than PA75 and PA25 scaffolds. However, PA50 scaffolds were structurally less stable than PA25 scaffolds, and a complete disintegration was noted after 8 weeks. This structural instability was related to the PLGA, which was present at the interface of PCL particles and removal of PLGA due to dissolution led the structure collapse.

In the current work, higher percentage weight loss is related to the degradation of the scaffold, mainly the PLGA5050 phase. This is also observed in Figure 5, where higher weight loss was noted in the case of higher PLGA5050 content samples. Furthermore, the rate of degradation was also higher in the case of high PLGA5050 content samples. It is worth mentioning here that in the presence of water, PLGA degrades via the hydrolysis of its ester linkages. At 6 weeks, all PLGA5050 present in each group (75 wt.% in PA75, 50 wt.% in PLA50, and 25 wt.% in PA25) had already been dissolved (Figure 6A). This led to a decrease in the rate of degradation at 6 weeks of dissolution period and thereafter (Figure 6B). Based on the current study, PA50 scaffolds were found promising for the load-bearing bone tissue engineering applications due to their relatively high mechanical properties and low degradation rates than those of PA75. Furthermore, as compared to PA75 and PA 25, the

highest percentage porosity was noted in PA50 scaffolds, which can be helpful in the vascularization.

In this investigation, no attempt was made to generate functionally-graded scaffolds. The use of various fabrication methods to generate gradients in porosity, bioactive concentrations and mechanical properties in the axial and transverse directions has the potential to further optimize scaffold structures, mechanical properties and bioactive concentrations for the treatment and repair of critical-sized bone defects [40–46]. Such methods can be tailored using the results of this investigation as to what the PCL/PLGA ratio needs to be at various radial and axial locations of the scaffolds and bone graft substitutes.

5. Conclusions

The present study reports the optimization of PCL and PLGA5050 ratio to design a biodegradable scaffold for the load-bearing orthopedic applications. The incorporation of PLGA5050 in PCL matrix led to an increase in the degradation rate of the scaffold and formation of in-situ pores upon degradation of PLGA. SEM studied revealed a strong interface between the PCL and PLGA phases. This was helpful in the improvement of scaffold strength. Furthermore, a strong effect of PLGA on the mechanical behavior of the sample was found during the compression testing which was related to the glass transition temperature of the PLGA which is above the room temperature.

Supplementary Material

Refer to Web version on PubMed Central for supplementary material.

Acknowledgments

The work was partly supported by the National Institute of Biomedical Imaging and Bioengineering of the National Institutes of Health (award number R01EB020640), and the Assistant Secretary of Defense for Health Affairs, through the Peer Reviewed Medical Research Program under Award No. W81XWH-16-1-0132. We gratefully acknowledge Mr. Agrim Mahajan for his help in sample preparation.

References

1. Leppik L, Zhihua H, Mobini S, et al. Combining electrical stimulation and tissue engineering to treat large bone defects in a rat model. Scientific Reports. 2018;8(1):6307–6320. [PubMed: 29679025]
2. Schemitsch EH. Size Matters: Defining Critical in Bone Defect Size! Journal of Orthopaedic Trauma. 2017;31:S20–S22.
3. Begley CT, Doherty MJ, Mollan RAB, Wilson JD. Comparative study of the osteoinductive properties of bioceramic, coral and processed bone graft substitutes. Biomaterials. 1995;16:1181–1185. [PubMed: 8562796]
4. Silva RV, Camilli JA, Bertran CA, Moreira NH. The use of hydroxyapatite and autogenous cancellous bone grafts to repair bone defects in rats. International Journal of Oral and Maxillofacial Surgery. 2004;10:1–7.
5. Whang PG, Wang JC. Bone graft substitutes for spinal fusion. The Spine Journal. 2003;3:155–165. [PubMed: 14589231]
6. Vaccaro AR. The role of the osteoconductive scaffold in synthetic bone graft. Orthopedics. 2002;25:571–278.
7. Bonfiglio M, Jeter WS. Immunological responses to bone. Clinical Orthopaedics. 1972;18:19–27.

8. GD GDB, Goldberg VM, Zika JM. Immune responses of rats to frozen bone allografts. Journal of Bone & Joint Surgery, American Volume. 1983;65-A:239–246.
9. O'Malley MJ, Sayres SC, Saleem O, et al. Morbidity and complications following percutaneous calcaneal autograft bone harvest. Foot and Ankle Internataional. 2014;35:30–37.
10. Surmenev RA, Surmeneva MA, Ivanova AA. Significance of calcium phosphate coatings for the enhancement of new bone osteogenesis–A review. Acta Biomaterialia. 2014;10(2):557–579. [PubMed: 24211734]
11. Bose S, Vahabzadeh S, Bandyopadhyay A. Bone tissue engineering using 3D printing. Materials Today. 2013;16(12):496–504.
12. Polo-Corrales L, Latorre-Esteves M, Ramirez-Vick JE. Scaffold design for bone regeneration. Journal of nanoscience and nanotechnology. 2014;14(1):15–56. [PubMed: 24730250]
13. Hollister SJ. Porous scaffold design for tissue engineering. Nature Materials. 2005;4(7):518. [PubMed: 16003400]
14. Kumar A, Nune KC, Misra RDK. Biological functionality and mechanistic contribution of extracellular matrix-ornamented three dimensional Ti-6Al-4V mesh scaffolds. Journal of Biomedical Materials Research Part A. 2016;104(11):2751–2763. [PubMed: 27325185]
15. Kumar A, Nune KC, Misra RDK. Design and biological functionality of a novel hybrid Ti-6 A l-4 V/hydrogel system for reconstruction of bone defects. Journal of Tissue Engineering and Regenerative Medicine. 2018;12(4):1133–1144. [PubMed: 29134773]
16. Hernandez I, Kumar A, Joddar B. A Bioactive Hydrogel and 3D Printed Polycaprolactone System for Bone Tissue Engineering. Gels. 2017;3(3):26. [PubMed: 29354645]
17. Hollander DA, von Walter M, Wirtz T, et al. Structural, mechanical and in vitro characterization of individually structured Ti–6Al–4V produced by direct laser forming. Biomaterials. 2006/03/01/ 2006;27(7):955–963. [PubMed: 16115681]
18. Pattanayak DK, Fukuda A, Matsushita T, et al. Bioactive Ti metal analogous to human cancellous bone: Fabrication by selective laser melting and chemical treatments. Acta Biomaterialia. 2011/03/01/ 2011;7(3):1398–1406. [PubMed: 20883832]
19. Matsushita T, Fujibayashi S, Kokubo T. 4 - Titanium foam for bone tissue engineering In: Wen C, ed. Metallic Foam Bone: Woodhead Publishing; 2017:111–130.
20. Hong D, Chou D-T, Velikokhatnyi OI, et al. Binder-jetting 3D printing and alloy development of new biodegradable Fe-Mn-Ca/Mg alloys. Acta Biomaterialia. 2016/11/01/ 2016;45:375–386. [PubMed: 27562611]
21. Chen Q, Thouas GA. Metallic implant biomaterials. Materials Science and Engineering: R: Reports. 2015/01/01/ 2015;87:1–57.
22. Lu J, Descamps M, Dejou J, et al. The biodegradation mechanism of calcium phosphate biomaterials in bone. Journal of Biomedical Materials Research: An Official Journal of The Society for Biomaterials, The Japanese Society for Biomaterials, and The Australian Society for Biomaterials and the Korean Society for Biomaterials. 2002;63(4):408–412.
23. Chen QZ, Thompson ID, Boccaccini AR. 45S5 Bioglass®-derived glass–ceramic scaffolds for bone tissue engineering. Biomaterials. 2006;27(11):2414–2425. [PubMed: 16336997]
24. Kumar A, Akkineni AR, Basu B, Gelinsky M. Three-dimensional plotted hydroxyapatite scaffolds with predefined architecture: Comparison of stabilization by alginate cross-linking versus sintering. Journal of biomaterials applications. 2016;30(8):1168–1181. [PubMed: 26589296]
25. Seyednejad H, Gawlitta D, Kuiper RV, et al. In vivo biocompatibility and biodegradation of 3D-printed porous scaffolds based on a hydroxyl-functionalized poly (ε-caprolactone). Biomaterials. 2012;33(17):4309–4318. [PubMed: 22436798]
26. Nazarov R, Jin H-J, Kaplan DL. Porous 3-D scaffolds from regenerated silk fibroin. Biomacromolecules. 2004;5(3):718–726. [PubMed: 15132652]
27. Deng M, Nair LS, Nukavarapu SP, et al. In situ porous structures: a unique polymer erosion mechanism in biodegradable dipeptide-based polyphosphazene and polyester blends producing matrices for regenerative engineering. Advanced Functional Materials. 2010;20(17):2794–2806.
28. Hiep NT, Lee B-T. Electro-spinning of PLGA/PCL blends for tissue engineering and their biocompatibility. J Mater Sci: Mater Med. 2010;21(6):1969–1978. [PubMed: 20232234]

29. Kim JY, Cho D-W. Blended PCL/PLGA scaffold fabrication using multi-head deposition system. Microelectronic Engineering. 2009;86(4–6):1447–1450.
30. Raspa A, Marchini A, Pugliese R, et al. A biocompatibility study of new nanofibrous scaffolds for nervous system regeneration. Nanoscale. 2016;8(1):253–265. [PubMed: 26607419]
31. Patrício T, Bártolo P. Thermal stability of PCL/PLA blends produced by physical blending process. Procedia Engineering. 2013;59:292–297.
32. Qian Y, Zhang Z, Zheng L, Song R, Zhao Y. Fabrication and characterization of electrospun polycaprolactone blended with chitosan-gelatin complex nanofibrous mats. Journal of Nanomaterials. 2014;2014:1.
33. Guo W, Quan P, Fang L, Cun D, Yang M. Sustained release donepezil loaded PLGA microspheres for injection: Preparation, in vitro and in vivo study. asian journal of pharmaceutical sciences. 2015;10(5):405–414.
34. Woodruff MA, Hutmacher DW. The return of a forgotten polymer—polycaprolactone in the 21st century. Progress in polymer science. 2010;35(10):1217–1256.
35. Chew SA, Arriaga MA, Hinojosa VA. Effects of surface area to volume ratio of PLGA scaffolds with different architectures on scaffold degradation characteristics and drug release kinetics. Journal of Biomedical Materials Research Part A. 2016;104(5):1202–1211. [PubMed: 26780154]
36. Bružauskaitė I, Bironaitė D, Bagdonas E, Bernotienė E. Scaffolds and cells for tissue regeneration: different scaffold pore sizes—different cell effects. Cytotechnology. 2016;68(3):355–369. [PubMed: 26091616]
37. Murugan R, Ramakrishna S. Development of nanocomposites for bone grafting. Composites Science and Technology. 2005;65(15–16):2385–2406.
38. Gittens RA, McLachlan T, Olivares-Navarrete R, et al. The effects of combined micron-/submicron-scale surface roughness and nanoscale features on cell proliferation and differentiation. Biomaterials. 2011;32(13):3395–3403. [PubMed: 21310480]
39. Rouwkema J, Rivron NC, van Blitterswijk CA. Vascularization in tissue engineering. TRENDS in Biotechnology. 2008;26(8):434–441. [PubMed: 18585808]
40. Ozkan S, Kalyon DM, Yu X, McKelvey CA, Lowinger M. Multifunctional protein-encapsulated polycaprolactone scaffolds: fabrication and in vitro assessment for tissue engineering. Biomaterials. 2009;30(26):4336–4347. [PubMed: 19481253]
41. Ozkan S, Kalyon DM, Yu X. Functionally graded b-TCP/PCL nanocomposite scaffolds for bone tissue engineering: in vitro evaluation with human fetal osteoblast cells. J Biomed Mater Res A. 2010;92:1007. [PubMed: 19296543]
42. Ergun A, Yu X, Valdevit A, Ritter A, Kalyon DM. In vitro analysis and mechanical properties of twin screw extruded single-layered and coextruded multilayered poly (caprolactone) scaffolds seeded with human fetal osteoblasts for bone tissue engineering. Journal of Biomedical Materials Research Part A. 2011;99(3):354–366. [PubMed: 22021183]
43. Ergun A, Yu X, Valdevit A, Ritter A, Kalyon DM. Radially and axially graded multizonal bone graft substitutes targeting critical-sized bone defects from polycaprolactone/hydroxyapatite/tricalcium phosphate. Tissue Engineering Part A. 2012;18(23–24):2426–2436. [PubMed: 22764839]
44. Kalyon DM, Yu X, Wang H, Valdevit A, Ritter A. Twin Screw Extrusion Based Technologies Offer Novelty, Versatility, Reproducibility and Industrial Scalability for Fabrication of Tissue Engineering Scaffolds. J. Tissue Sci. Eng 2013;4(2):2–3.
45. Kalyon DM, Erisken C, Ozkan S, et al. Functionally-graded polymeric graft substitutes and scaffolds for tissue engineering can be fabricated via various extrusion methods. Journal of Tissue Science & Engineering. 2014;5(1):1.
46. Chung R, Kalyon DM, Yu X, Valdevit A. Segmental bone replacement via patient-specific, three-dimensional printed bioresorbable graft substitutes and their use as templates for the culture of mesenchymal stem cells under mechanical stimulation at various frequencies. Biotechnology and bioengineering. 2018;115(9):2365–2376. [PubMed: 29940090]

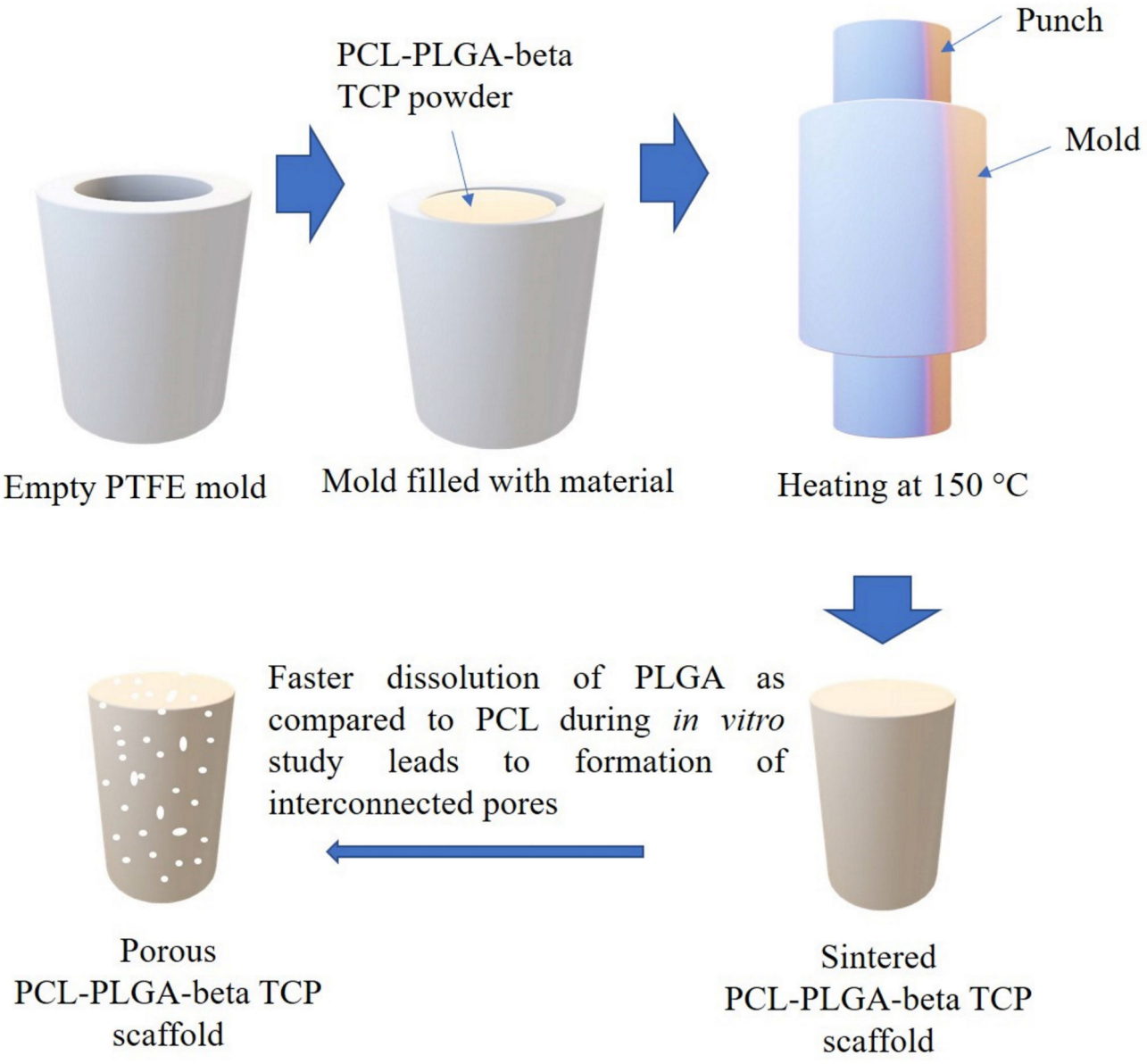

Figure 1:
Schematic of the fabrication process of PCL-PLGA-βTCP scaffolds and formation of pores due to the dissolution of PLGA5050 from the PCL matrix.

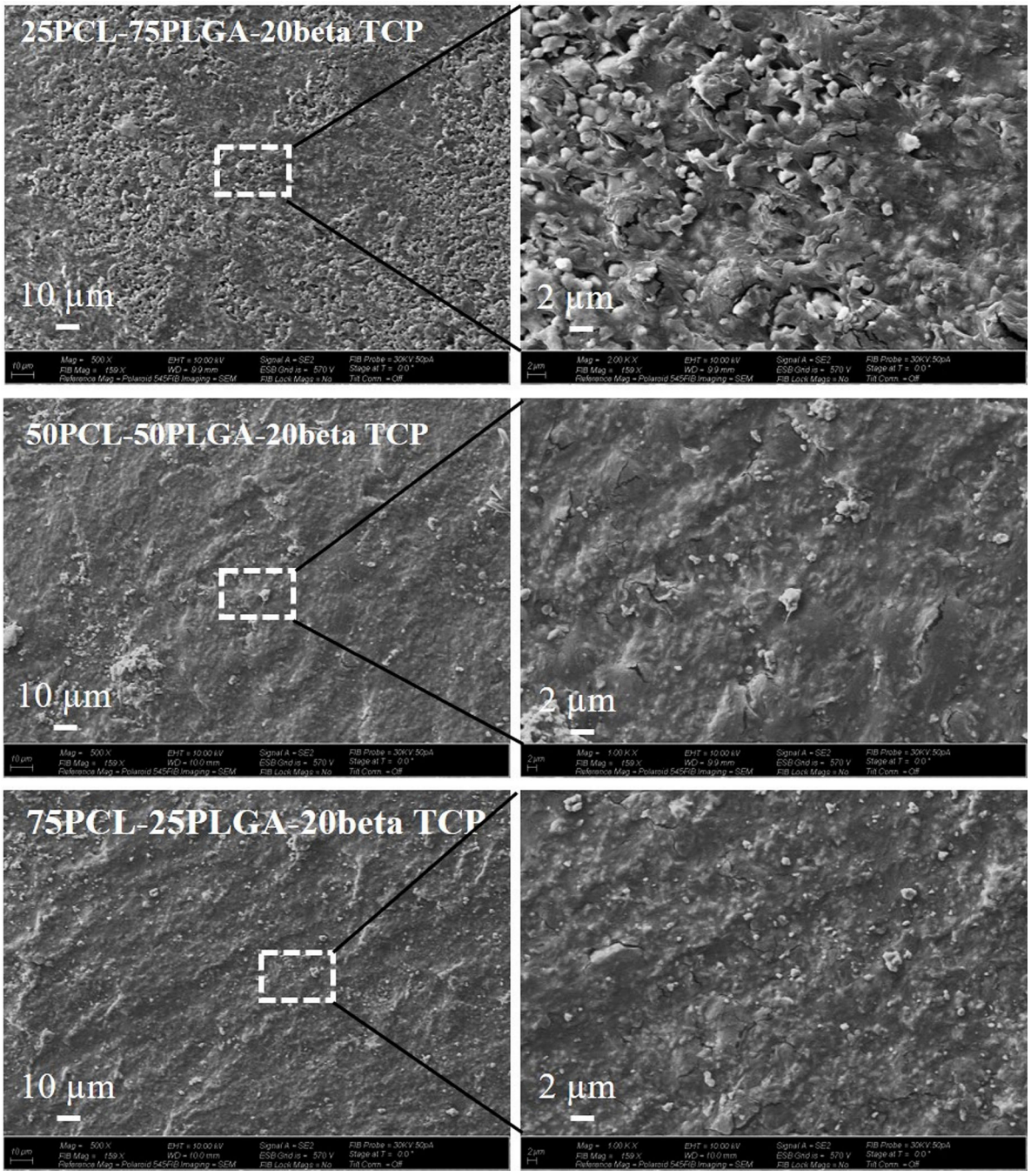

Figure 2:

Representative secondary electron microscopy micrographs are showing rough surface in high PLGA content samples and relatively smoother surface in case of low PLGA content samples. Higher magnification images confirmed the presence of microcracks in the as-prepared samples.

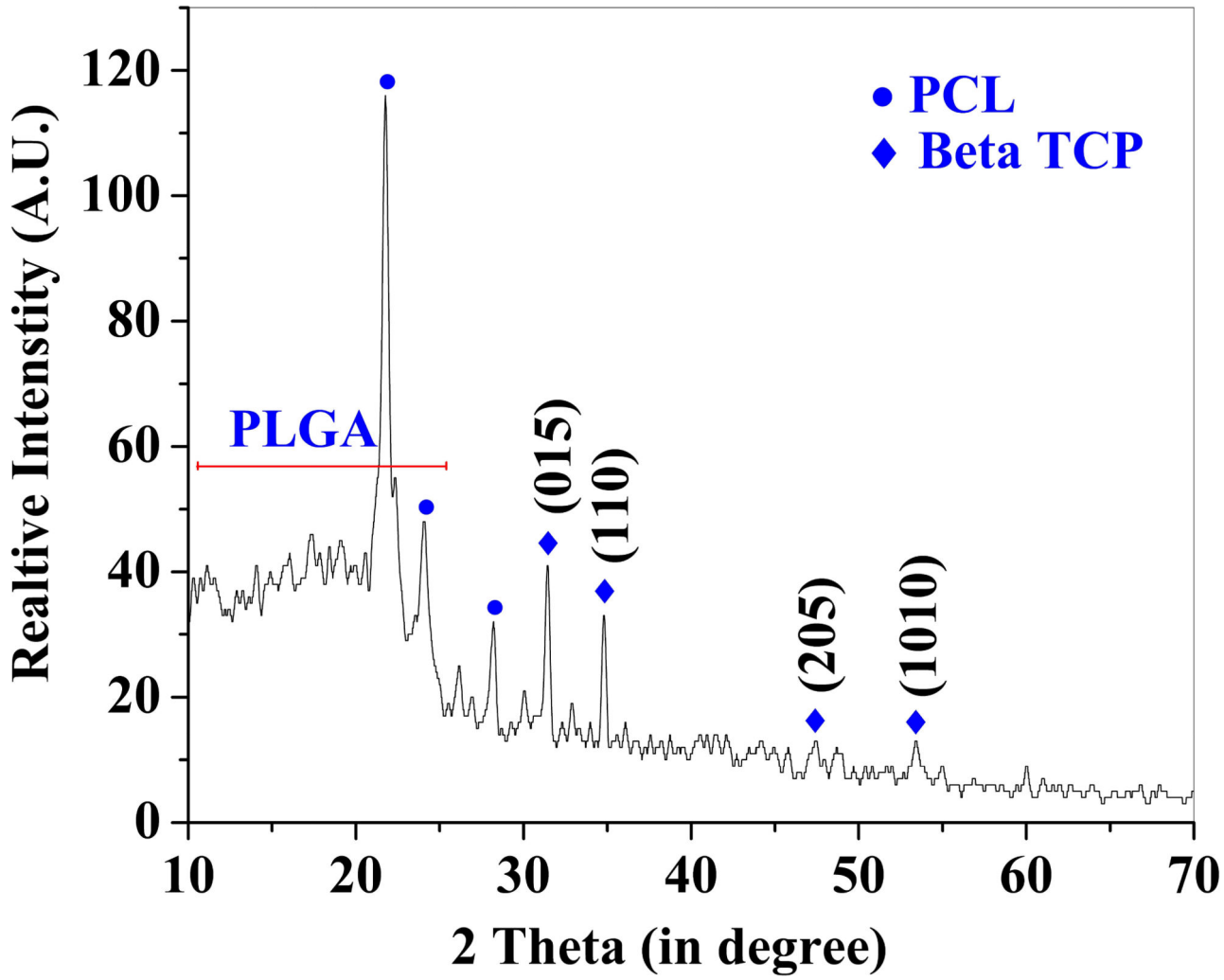

Figure 3:

Representative X-ray diffraction results confirmed the presence of PCL, PLGA, and βTCP in the as-sintered 50PCL-50PLGA-20βTCP. The sharp diffraction peaks related to the PCL and βTCP confirmed their crystalline nature. The PLGA was confirmed as an amorphous phase with a broad diffraction peak.

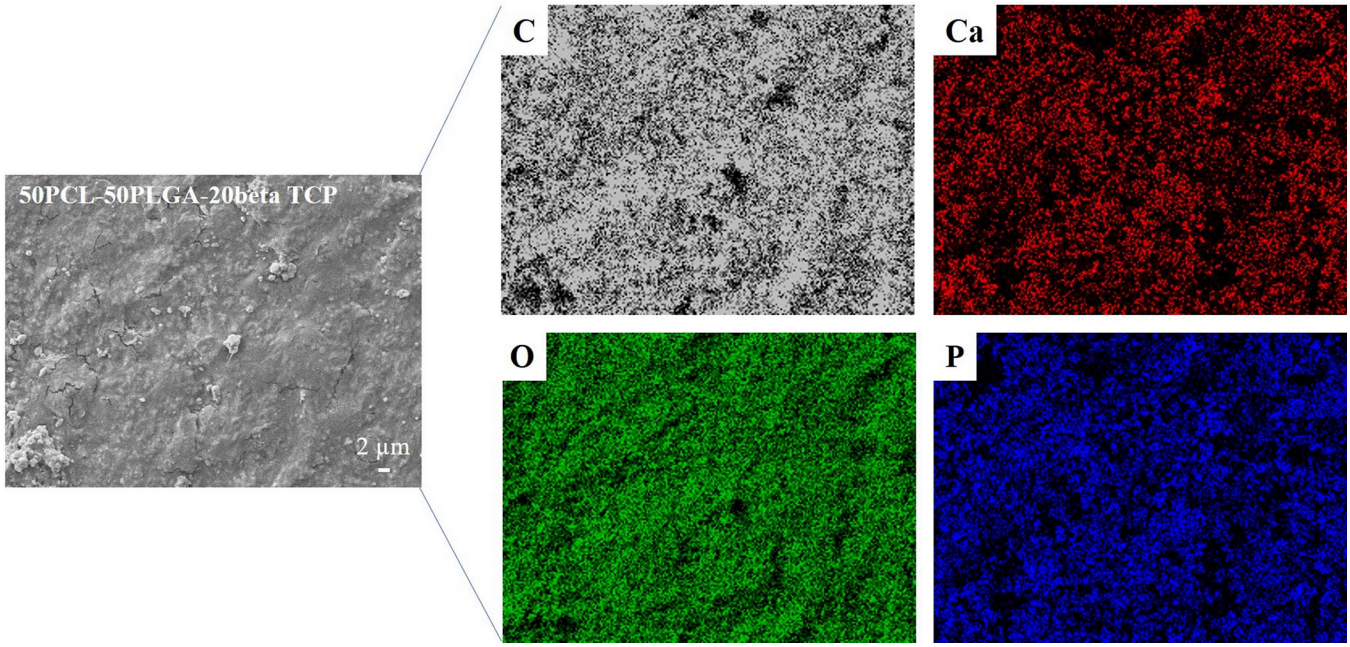

Figure 4:

Results of EDS elemental mapping showing the presence of C which is related to the PCL/PLGA phase. The Ca, P, and O are related to the βTCP particles, uniformly distributed in the polymeric matrix (50PCL-50PLGA).

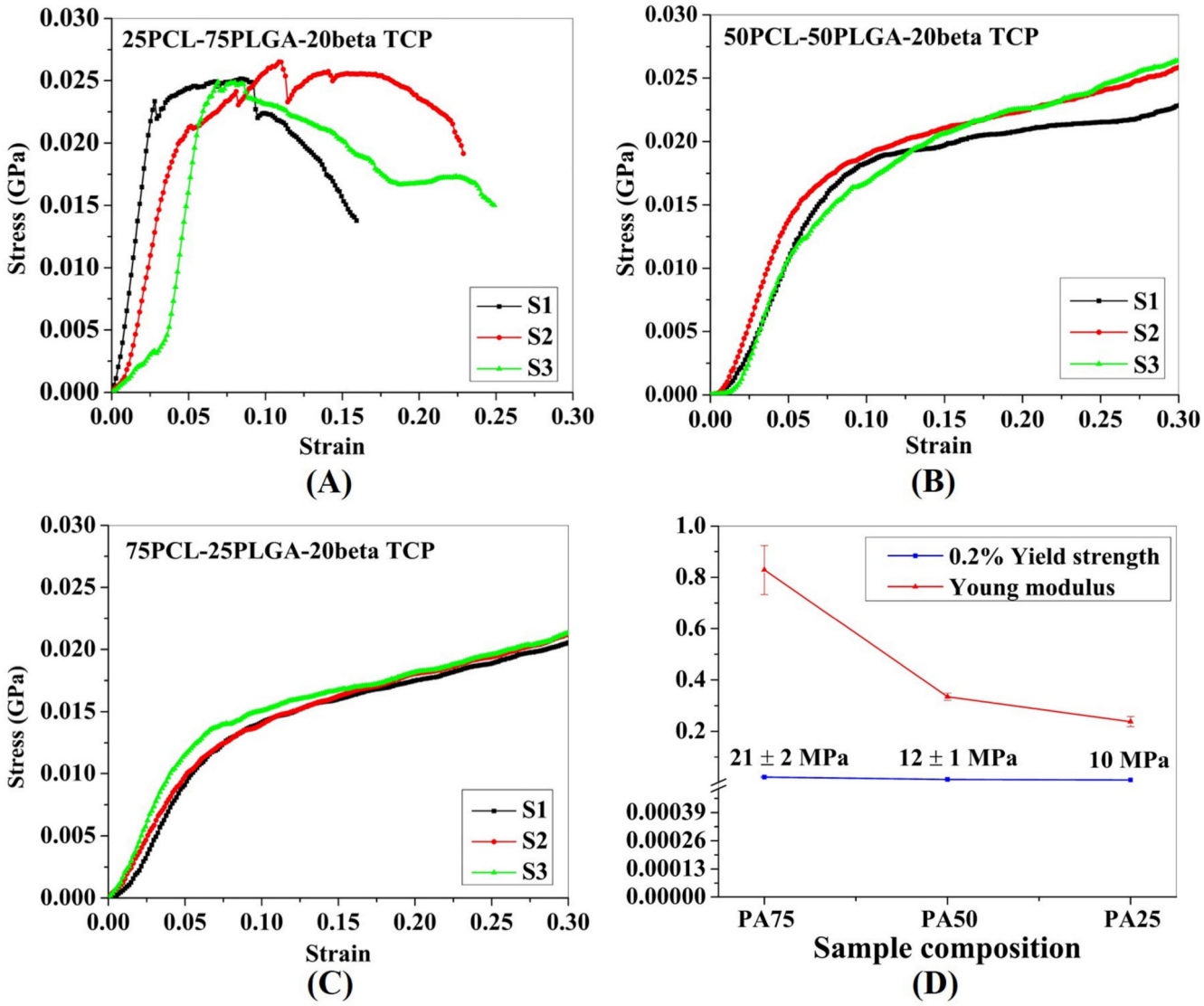

Figure 5:

Results of compression testing of (A) 25PCL-75PLGA-βTCP, (B) 50PCL-50PLGA-βTCP, and (C) 75PCL-25PLGA-βTCP. (D) Effect of PLGA and PCL ratio on the 0.2% yield strength and Young modulus. The lower mechanical properties were found due to the decrease in the PLGA content in the PCL/PLGA samples.

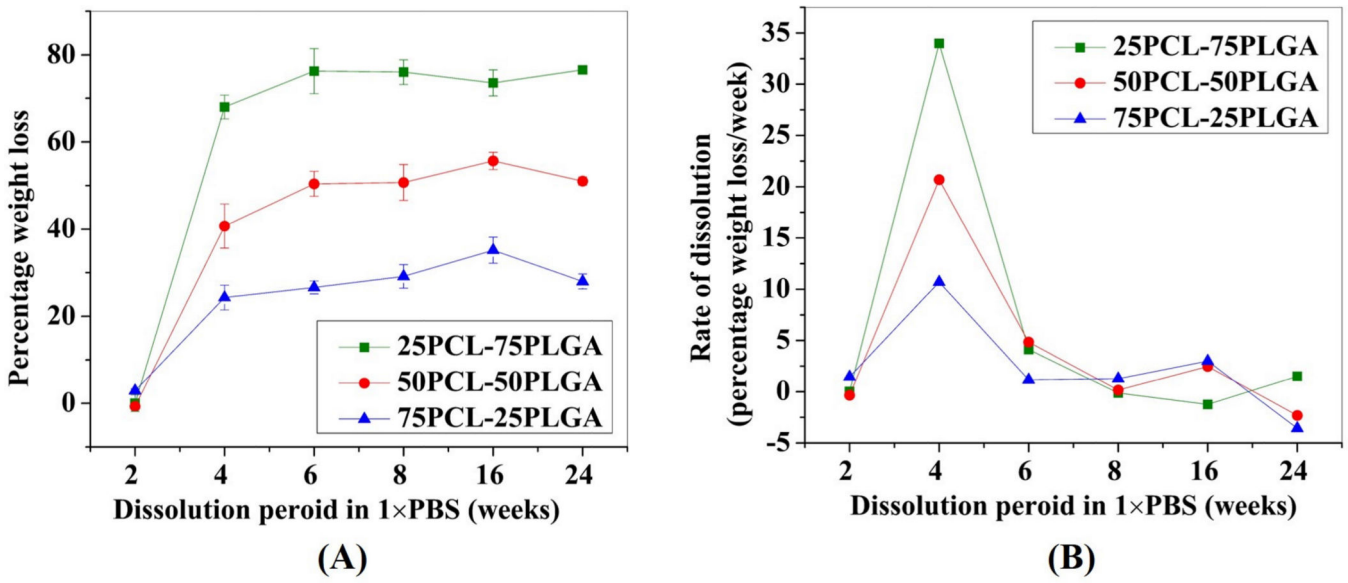

Figure 6:

Effect of PLGA amount on the (A) degradation behavior and (B) degradation rate of PCL-PLGA- βTCP scaffolds. The higher PLGA content in PCL/PLGA samples resulted in higher weight loss and degradation rate during the dissolution study in 1×PBS.

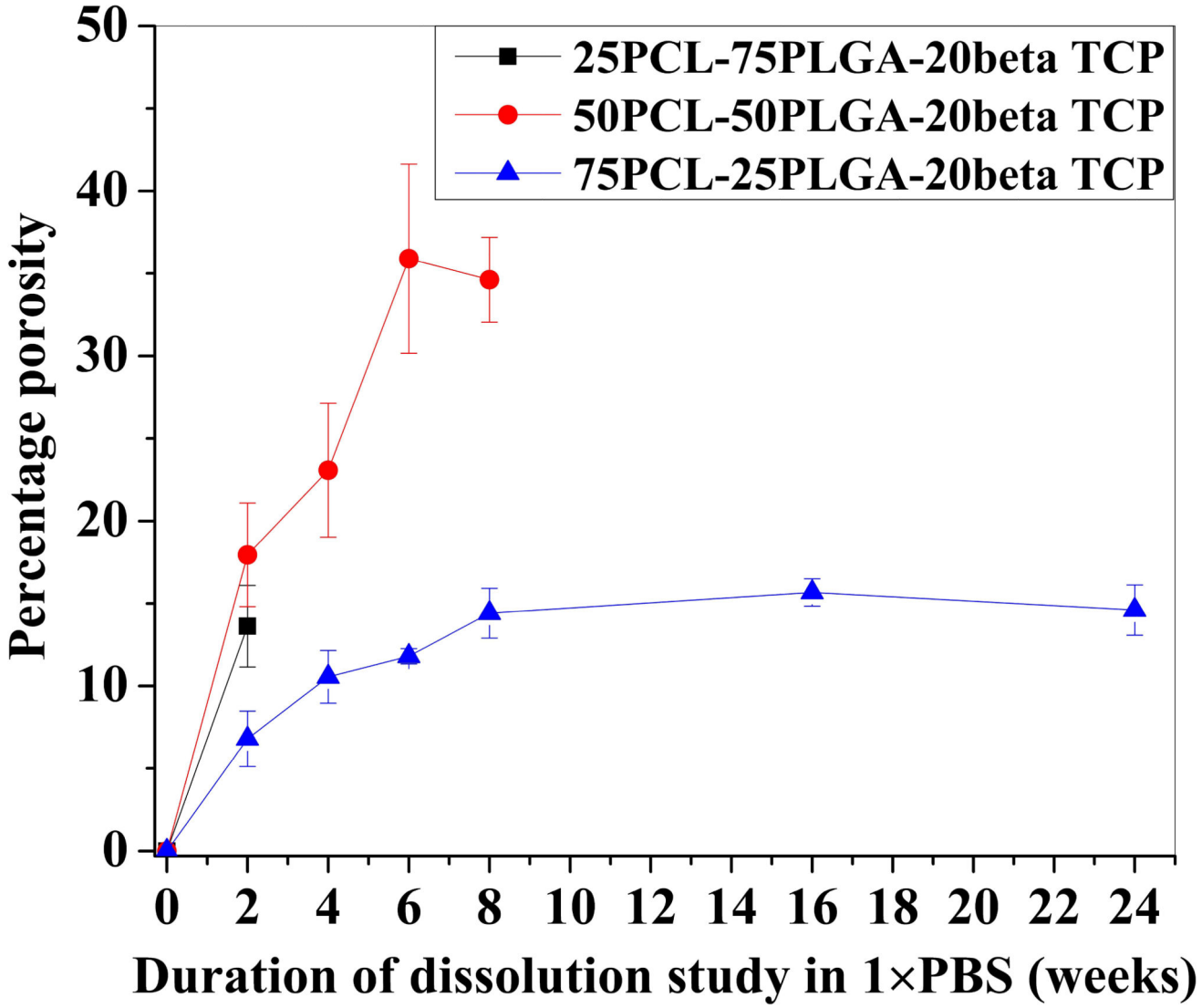

Figure 7:
Effect of dissolution time on the porosity. In the case of 25PCL-75PLGA-20βTCP and 50PCL-50PLGA-20βTCP compositions, samples were disintegrated due to extensive degradation after 2 and 8 weeks in 1×PBS, respectively.